A Bandpass Wavelet OFDM System for Power Line Communications

Freddy A. Pinto–Benel[a,*], Fernando Cruz–Roldán[a]

[a]*Department of Teoría de la Señal y Comunicaciones, Escuela Politécnica Superior. Universidad de Alcalá. 28871 Alcalá de Henares, SPAIN*

Abstract

A bandpass wavelet OFDM system, based on the time-domain waveform signals described in the standard IEEE Std. 1901-2010 for broadband power line communications, is presented. Several important aspects of the bandpass physical layer are reviewed, focusing on the scheme of modulation. Furthermore, a viable receiver system that is compatible with the transmitter and that also includes an equalizer system, is proposed. This paper also derives theoretical expressions for different powers at the receiver side, corresponding to the desired signal, as well as to the intersymbol and the intercarrier interference, and the noise. With these expressions, the signal-to-interference plus noise ratio and the achievable data rate of wavelet OFDM for bandpass communications are calculated. Finally, several computer simulations complete this work, assuming different PLC scenarios.

Keywords: power line communications (PLC), Internet of Things (IoT), wavelet OFDM, multicarrier modulation (MCM), filter bank multicarrier (FBMC), extended lapped transform (ELT), IEEE 1901.

1. Introduction

It is expected that power line communications (PLC) will play an important role in development of smart energy and the smart grid [1, 2, 3, 4, 5, 6]. These two concepts seek to boost the energy generation and transmission efficiency, providing real-time monitoring and control as well as information about energy demand. In this context, there are several applications of PLC from high voltage lines to in-home electrical wiring [1].

In addition, the urban Internet of Things (IoT) may provide a detailed view about the energy consumption within a city [4, 5, 6]. By means of IoT, consumers can directly control and manage their power consumption to different

---

*Corresponding author

Email addresses: `freddy.pinto@uah.es` (Freddy A. Pinto–Benel),
`fernando.cruz@uah.es` (Fernando Cruz–Roldán)

energy prices throughout then allowing them to save money. They can even produce their own energy and sell the excess to the grid. For this in-home IoT connection, the power line provides an attractive communication medium [7, 6] and PLC has become a competitive candidate technology to provide high-speed coverage using existing infrastructure [8, 6].

The IEEE 1901.3 standard specifies Physical (PHY) and Media Access Control (MAC) layers of a broadband powerline communication technology for Internet of Things applications (IoTPLC), and it is based on wavelet Orthogonal Frequency Division Multiplexing (wavelet OFDM). Previously, the standard IEEE Std. 1901-2010 (IEEE 1901 [9]), deployed two different PHY, with windowed OFDM and wavelet OFDM. Windowed OFDM is widely deployed in both wireless and wireline communication standards, including those for PLC (IEEE 1901[9] and IEEE 1901.2[10]). However, the performance of windowed OFDM systems, based on the discrete Fourier transform (DFT), is degraded in noisy environments. In order to reduce the above, wavelet OFDM presents appealing features such as greater spectral separation, reduced adjacent subchannel interference, and it shows higher robustness in noisy environments. In addition, it can allow for higher data rate since the use of redundant data as the cyclic prefix (CP) can be avoided. Wavelet OFDM is deployed in [9] with two different procedures: baseband and bandpass. The baseband wavelet OFDM is studied in [11]. Specifically, it is shown that the baseband transmitter is based on an extended lapped transform (ELT), and some important characteristics of the prototype filter deployed by the standard, are also presented in [11]. Furthermore, a power line channel equalization method is derived and its performance is assessed by computer simulations.

Regarding the bandpass wavelet OFDM transmitter, it is proposed with the aim to keep spectral efficient for bandpass communications [9]. To best of our knowledge, no prior work has presented the aspects of the wavelet OFDM bandpass physical layer. The main contribution of this paper is the study and proposal of a transmitter and a receiver bandpass wavelet OFDM systems for broadband PLC. This paper is also intended to present the theoretical expressions to calculate the signal-to-interference plus noise ratio (SINR). These expressions are used to obtain the achievable data rate of the bandpass wavelet OFDM, considering an Adaptive Sine-modulated/Cosine-modulated filter bank Equalizer for Transmultiplexer (ASCET) as equalization technique. To prove the feasibility of the system, its performance has been evaluated assuming different in-home PLC scenarios.

The rest of this paper is organized as follows. In Section 2, the modulation scheme of the transceiver is presented. In Section 3, theoretical expressions for the power of the desired signal, the power of the inter-symbol interference (ISI) and of the inter-carrier interference (ICI), and the power of the noise, all at the receiver side, are derived. From these expressions, the SINR and the achievable data rate are obtained. Section 4 provides the performance evaluation of the wavelet OFDM bandpass system. Finally, Section 5 provides our conclusions.
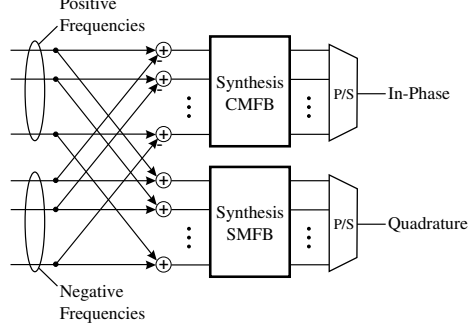
Figure 1: Block diagram of the passband transmitter deployed by the standard [9, Figure 14-26].

2. Filter Bank Multicarrier System

2.1. Transmitting System

Fig. 1 depicts the block diagram of the bandpass transmitter scheme shown in [9, Figure 14-26]. The in-phase $S^I[n]$ and quadrature $S^Q[n]$ time-domain waveform signals for the frame body are stated in [9, p. 1200] as follows:

$$
\begin{aligned}
S^I[n] = \frac{1}{16} & \left[\sum_{m=0}^{3} \sum_{k \in K_{on}} x_{m,k}^+ \cdot p[n + Mm] \right. \\
& \left. \times \cos\left(\frac{\pi}{M}\left((n + Mm) + \frac{M+1}{2} \right)\left(k + \frac{1}{2} \right) + \theta_k \right) \right] \\
- \frac{1}{16} & \left[\sum_{m=0}^{3} \sum_{k \in K_{on}} x_{m,k}^- \cdot p[n + Mm] \right. \\
& \left. \times \sin\left(\frac{\pi}{M}\left((n + Mm) + \frac{M+1}{2} \right)\left(k + \frac{1}{2} \right) + \theta_k \right) \right],
\end{aligned}
\tag{1a}
$$

$$
\begin{aligned}
S^Q[n] = \frac{1}{16} & \left[\sum_{m=0}^{3} \sum_{k \in K_{on}} x_{m,k}^+ \cdot p[n + Mm] \right. \\
& \left. \times \cos\left(\frac{\pi}{M}\left((n + Mm) + \frac{M+1}{2} \right)\left(k + \frac{1}{2} \right) + \theta_k \right) \right] \\
+ \frac{1}{16} & \left[\sum_{m=0}^{3} \sum_{k \in K_{on}} x_{m,k}^- \cdot p[n + Mm] \right. \\
& \left. \times \sin\left(\frac{\pi}{M}\left((n + Mm) + \frac{M+1}{2} \right)\left(k + \frac{1}{2} \right) + \theta_k \right) \right],
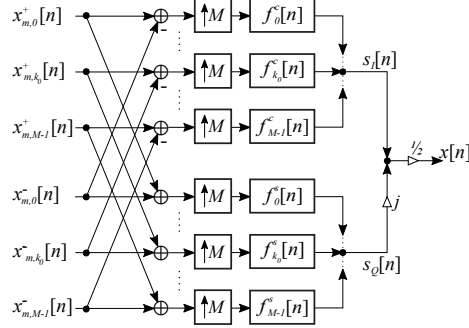\end{aligned}
\tag{1b}
$$

Figure 2: General block diagram of the bandpass wavelet OFDM transmitter.

where $0 \leq n < M$, M denotes the number of subcarriers, $\mathbb{K}_{on} \subseteq \{0, \ldots, M-1\}$ is the set of active subchannels[1] defined by the tone mask [9], and θ_k is a phase constant for peak power reduction. The carrier data on positive and negative frequencies relative to the bandpass carrier are denoted by positive x^+ and negative x^- superscripts. The values of θ_k, equal 0 or π, are defined in [9, Table 14-10] for $M = 512$. As with the baseband system, the standard [9] deploys for bandpass communications prototype filters $p[n]$ that can have different lengths: $N = 2\kappa M$, with $\kappa = 2, 3$, and different number of subcarriers ($M = 512, 1024, 2048$). An in-depth study of the prototype filters can be found in [11, 12].

In (1), $m = 2\kappa$, i.e, an overlapping factor $\kappa = 2$ is assumed. In these conditions, (1a) and (1b) can be rewritten as:

$$S^I[n] = \sum_{m \in \mathbb{Z}} \sum_{k \in \mathbb{K}_{on}} \left(x_{m,k}^+ \cdot f_k^c[n - mM] - x_{m,k}^- \cdot f_k^s[n - mM] \right), \qquad (2a)$$

$$S^Q[n] = \sum_{m \in \mathbb{Z}} \sum_{k \in \mathbb{K}_{on}} \left(x_{m,k}^+ \cdot f_k^c[n - mM] + x_{m,k}^- \cdot f_k^s[n - mM] \right), \qquad (2b)$$

where

$$f_k^c[n] = \sqrt{\frac{2}{M}} p[n] \cos \left[\left(\frac{\pi}{M} \left(k + \frac{1}{2} \right) \left(n + \frac{M+1}{2} \right) \right) \right] \cos(\theta_k), \qquad (3a)$$

$$f_k^s[n] = \sqrt{\frac{2}{M}} p[n] \sin \left[\left(\frac{\pi}{M} \left(k + \frac{1}{2} \right) \left(n + \frac{M+1}{2} \right) \right) \right] \cos(\theta_k), \qquad (3b)$$

Notice that θ_k only affects the sign of the time-domain waveform. In addition, the scale factor $\frac{1}{16}$ matches with $\sqrt{\frac{2}{M}}$ for $M = 512$.

---

[1] The index k is defined into the range of $[0, M-1]$ for the positive or negative subbands.
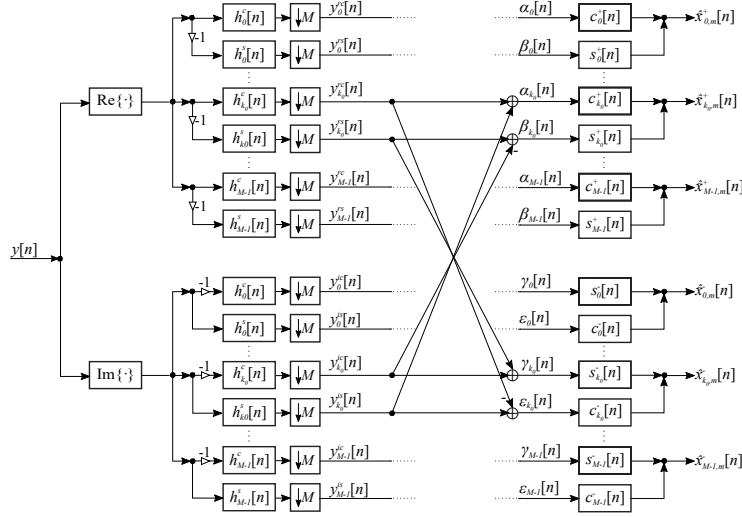
Figure 3: Block diagram of the bandpass wavelet OFDM receiver with ASCET.

Fig. 2 shows the block diagram of the proposed transmitter that obtains the time-domain waveform signals stated by the standard. The functions $f_k^c[n]$ and $f_k^s[n]$ are, respectively, the synthesis filters of a cosine modulated filter bank (CMFB) and a sine modulated filter bank (SMFB) of an ELT. The set of both systems constitutes the synthesis or transmitting filters of an exponentially ELT, where [13]

$$f_k[n] = f_k^c[n] + j \cdot f_k^s[n] = \sqrt{\frac{2}{M}} p[n] e^{j \cdot \left(\frac{\pi}{M} \left(k + \frac{1}{2} \right) \left(n + \frac{M+1}{2} \right) \right)} \cdot \cos(\theta_k). \quad (4)$$

Taking into account the studies performed in [14, 15, 16], the kth complex synthesis filter can be expressed as

$$f_k^\pm[n] = \pm f_k^c[n] + j \cdot f_k^s[n], \quad (5)$$

where the positive signs stand for positive bandpass frequencies and the negative signs stand for negative frequencies.

2.2. Receiving System

The previous transmitting bank leads us to propose the compatible receiver of Fig. 3 to demodulate the transmitted data and to equalize the channel. Let us consider first the following impulse responses:

$$h_k[n] = \sqrt{\frac{2}{M}} p[n] e^{j \cdot \left(\frac{\pi}{M} \left(k + \frac{1}{2} \right) \left(N - 1 - n + \frac{M+1}{2} \right) \right)} \cdot \cos(\theta_k). \quad (6)$$

We then define

$$\begin{aligned} h_k^\pm[n] &= \pm h_k^c[n] - j \cdot h_k^s[n] \\ &= \pm f_k^c[N-1-n] - j \cdot f_k^s[N-1-n], \end{aligned} \quad (7)$$

5

where the k-th complex analysis filter can be implemented as the time reflection of the transmission bank

$$h_k^c[n] = \sqrt{\frac{2}{M}} \cdot p[n] \cdot \cos\left[\left(\frac{\pi}{M}\left(k + \frac{1}{2}\right)\right)\left(N - 1 - n + \frac{M+1}{2}\right)\right] \cdot \cos\left(\theta_k\right),$$

$$h_k^s[n] = \sqrt{\frac{2}{M}} \cdot p[n] \cdot \sin\left[\left(\frac{\pi}{M}\left(k + \frac{1}{2}\right)\right)\left(N - 1 - n + \frac{M+1}{2}\right)\right] \cdot \cos\left(\theta_k\right).$$

The block diagram of Fig. 3 also includes an Adaptive Sine-modulated/Cosine-modulated filter bank Equalizer for Transmultiplexer (ASCET) [17, 18, 16, 11]. The simplest equalization system is the 0-ASCET, in which the filters $c_k^\pm[n]$ and $s_k^\pm[n]$ are constants. That is, the transmission channel effects are compensated for by multiplying each output of the real and imaginary cosine/sine modulated receiving filter bank, respectively, by the constant numbers $c_k^\pm$ and $s_k^\pm$:

$$E_k(\Omega)|_{\Omega=(2k+1)\frac{2\pi}{4M}} = c_k^+ - js_k^+ \tag{9a}$$

$$E_{M+k}(\Omega)|_{\Omega=(2(M+k)+1)\frac{2\pi}{4M}} = c_{M-1-k}^- - js_{M-1-k}^- \tag{9b}$$

for $0 \leq k \leq M - 1$. These constants $c_k^\pm$ and $s_k^\pm$ are the real and the imaginary part of E_k and E_{2M-1-k}, respectively, which can be calculated, under additive white Gaussian noise (AWGN) [18], as follows

$$E_k\left(e^{j(2k+1)\frac{2\pi}{4M}}\right) = \frac{H_{ch}^*\left(e^{j(2k+1)\frac{2\pi}{4M}}\right)}{|H_{ch}\left(e^{j(2k+1)\frac{2\pi}{4M}}\right)|^2 + \frac{1}{\text{SNR}}}, \tag{10}$$

where $H_{ch}\left(e^{j\Omega}\right)$ is the channel frequency response and SNR is the signal-to-noise ratio, defined as the quotient of the input signal power to the noise power.

In general, however, the 0-ASCET is not enough to compensate for the power line channel distortion because there are fast variations within the subchannel bandwidth [11, 19]. Therefore, it is necessary to improve the performance by replacing the 0-ASCET for a $(2L + 1)$-tap FIR filter. These equalizers are called L-order ASCET or L-ASCET. Following the development presented in [20, 18, 16], the coefficients of the 1-ASCET (3-tap FIR) filter, for the positives and negatives subbands, can be obtained as

$$c_{i,k}^+ = \Re\{e_{i,k}\}, \tag{11a}$$

$$s_{i,k}^+ = -\Im\{e_{i,k}\}, \tag{11b}$$

$$c_{i,M-1-k}^- = \Re\{e_{i,M+k}\}, \tag{11c}$$

$$s_{i,M-1-k}^- = -\Im\{e_{i,M+k}\}, \tag{11d}$$

where $0 \leq k \leq M - 1$, $i = 0, 1, 2$, $\Re\{\cdot\}$ and $\Im\{\cdot\}$ stand for, respectively, the real

and the imaginary parts,

$$e_{0,k} = \pm \frac{1}{2} \left(\frac{\eta_{0,k} - \eta_{2,k}}{2} - j \left(\eta_{1,k} - \frac{\eta_{0,k} + \eta_{2,k}}{2} \right) \right), \qquad (12a)$$

$$e_{1,k} = \frac{\eta_{0,k} + \eta_{2,k}}{2}, \qquad (12b)$$

$$e_{2,k} = \pm \frac{1}{2} \left(\frac{\eta_{0,k} - \eta_{2,k}}{2} + j \left(\eta_{1,k} - \frac{\eta_{0,k} + \eta_{2,k}}{2} \right) \right), \qquad (12c)$$

and

$$\eta_{i,k} = \frac{H_{ch}^* \left(e^{j \frac{\pi}{4M}(2k+i)} \right)}{\left| H_{ch} \left(e^{j \frac{\pi}{4M}(2k+i)} \right) \right|^2 + \frac{1}{SNR}}. \qquad (13)$$

Note that the $\pm$ value of (12) must be chosen positive for the even subbands and negative for the odd ones.

If a higher order ASCET is required, then the expressions developed in [19] can be used to obtain a 2-ASCET (5-tap) system. However, increasing the order of the equalizer directly leads to an increase of the computational complexity for the receiver. Based on previous studies [11, 19, 12], the 2-ASCET seems to be a good choice.

3. Achievable Data Rate

This section discusses the expressions to determinate the theoretical throughput of a bandpass ELT-MCM system. This derivation is based on each transfer function that relates any input of the transmitter side to any output at the receiver side. A constellation of infinity granularity has been assumed, which means that each subcarrier can transport a fractional and unlimited number of bits.

The discrete-time transmitted signal in the z-domain can be expressed as follows

$$X(z) = S^I(z) + j \cdot S^Q(z), \qquad (14)$$

where

$$S^I(z) = \sum_{k \in \mathbb{K}_{on}} F_k^c(z) \left(X_k^+ \left(z^M \right) - X_k^- \left(z^M \right) \right) \qquad (15a)$$

$$S^Q(z) = \sum_{k \in \mathbb{K}_{on}} F_k^s(z) \left(X_k^+ \left(z^M \right) + X_k^- \left(z^M \right) \right) \qquad (15b)$$

and $F_k^c(z)$ and $F_k^s(z)$ are the system function of each filter given in (3a) and (3b), respectively. $X_k^+(z)$ ($X_k^-(z)$) is the symbol in the kth subcarrier of the positive (negative) subband, assumed to be zero-mean wide-sense stationary (WSS) process. In particular, the variance $\sigma_x^2(k)$ is assumed identical for all $X_k^\pm$ which are independent and identically distributed for every $k \in \mathbb{K}_{on}$. The different signals defined in (14) and (15) are plotted in the block diagram of Fig. 2.

7

Let us consider a complex channel impulse response and complex channel noise in the z-domain, respectively expressed as $H_{ch}(z) = H_{ch}^I(z) + j \cdot H_{ch}^Q(z)$ and $R(z) = R^I(z) + j \cdot R^Q(z)$. The first block in the receiver side must introduce a delay of β samples to obtain proper system operation. The general block of the wavelet OFDM receiver is depicted in Fig. 3. Therefore, the receiver signal can be written as

$$
\begin{aligned}
Y(z) &= X(z) \cdot H_{ch}(z) \cdot z^{-\beta} + R(z) \cdot z^{-\beta} \\
&= \Big[S^I(z) H_{ch}^I(z) - S^Q(z) H_{ch}^Q(z) \\
&\quad + j \Big(S^I(z) H_{ch}^Q(z) + S^Q(z) H_{ch}^I(z) \Big) \Big] \cdot z^{-\beta} + R(z) \cdot z^{-\beta} \quad (16)
\end{aligned}
$$

After the calculations in Appendix A, the reconstructed symbol can be calculated as follows

$$
\begin{aligned}
\hat{X}_i^+(z) = &X_i^+(z) \Upsilon_{i,i}'(z) + X_i^-(z) \Upsilon_{i,i}''(z) \\
&+ \sum_{\substack{k \in \mathbb{K}_{in} \\ k \neq i}} X_k^+(z) \Upsilon_{i,k}'(z) + \sum_{\substack{k \in \mathbb{K}_{in} \\ k \neq i}} X_k^-(z) \Upsilon_{i,k}''(z), \quad (17)
\end{aligned}
$$

$$
\begin{aligned}
\hat{X}_i^-(z) = &X_i^+(z) \Psi_{i,i}'(z) + X_i^-(z) \Psi_{i,i}''(z) \\
&+ \sum_{\substack{k \in \mathbb{K}_{in} \\ k \neq i}} X_k^+(z) \Psi_{i,k}'(z) + \sum_{\substack{k \in \mathbb{K}_{in} \\ k \neq i}} X_k^-(z) \Psi_{i,k}''(z), \quad (18)
\end{aligned}
$$

The expressions in the time-domain are

$$
\begin{aligned}
\hat{x}_i^+[n] &= \sum_\ell \big(v_{i,i}'[\ell] \cdot x_i^+[n - \ell] + v_{i,i}''[\ell] \cdot x_i^-[n - \ell] \big) \\
&\quad + \sum_{\substack{k \in \mathbb{K}_{in} \\ k \neq i}} \sum_\ell \big(v_{i,k}'[\ell] \cdot x_i^+[n - \ell] + v_{i,k}''[\ell] \cdot x_i^-[n - \ell] \big) \\
&= v_{i,i}'[0] \cdot x_i^+[n] + v_{i,i}''[0] \cdot x_i^-[n] \\
&\quad + \underbrace{\sum_{\substack{\ell \\ \ell \neq 0}} \big(v_{i,i}'[\ell] x_i^+[n - \ell] + v_{i,i}''[\ell] x_i^-[n - \ell] \big)}_{\text{ISI}} \\
&\quad + \underbrace{\sum_{\substack{k \in \mathbb{K}_{in} \\ k \neq i}} \sum_\ell \big(v_{i,k}'[\ell] \cdot x_i^+[n - \ell] + v_{i,k}''[\ell] \cdot x_i^-[n - \ell] \big)}_{\text{ICI}} \quad (19)
\end{aligned}
$$

8

$$
\begin{aligned}
\hat{x}_i^-[n] \;=\;& \psi'_{i,i}[0]\cdot x_i^+[n] + \psi''_{i,i}[0]\cdot x_i^-[n] \\
& + \underbrace{\sum_{\substack{\ell \\ \ell \neq 0}} \left(\psi'_{i,i}[\ell]x_i^+[n-\ell] + \psi''_{i,i}[\ell]x_i^-[n-\ell]\right)}_{\text{ISI}} \\
& + \underbrace{\sum_{\substack{k \in \mathbb{K}_{in} \\ k \neq i}} \sum_{\ell} \left(\psi'_{i,k}[\ell]\cdot x_i^+[n-\ell] + \psi''_{i,k}[\ell]\cdot x_i^-[n-\ell]\right)}_{\text{ICI}} \quad (20)
\end{aligned}
$$

where ISI and ICI denote, respectively, the intersymbol and the intercarrier interference.

Finally, the power of the ith subcarrier signal can be calculated as

$$
P_\gamma(i)^+ = \sigma_x^2 \left(\left|v'_{i,i}[0]\right|^2 + \left|v''_{i,i}[0]\right|^2 \right), \tag{21}
$$

$$
P_\gamma(i)^- = \sigma_x^2 \left(\left|\psi'_{i,i}[0]\right|^2 + \left|\psi''_{i,i}[0]\right|^2 \right). \tag{22}
$$

Similarly, the power corresponding to the intersymbol and intercarrier interference of the ith subcarrier ($P_{ISI}(i)$ and $P_{ICI}(i)$) can be obtained as

$$
\begin{aligned}
P_{\text{INT}}^+(i) = & P_{\text{ISI}}^+(i) + P_{\text{ICI}}^+(i) \\[2ex]
= & \sigma_x^2 \left(\sum_{\substack{\ell \\ \ell \neq 0}} \left(\left|v'_{i,i}[\ell]\right|^2 + \left|v''_{i,i}[\ell]\right|^2 \right) \right. \\[2ex]
& \left. + \sum_{\substack{k=0 \\ k \neq i}}^{M-1} \sum_{\ell} \left(\left|v'_{i,k}[\ell]\cdot\right|^2 + \left|v''_{i,k}[\ell]\cdot\right|^2 \right) \right),
\end{aligned}
\tag{23}
$$

$$P^-_{\mathrm{INT}}(i) = P^-_{\mathrm{ISI}}(i) + P^-_{\mathrm{ICI}}(i)$$

$$= \sigma_x^2 \left(\sum_{\substack{\ell \\ \ell \neq 0}} \left(\left| \psi'_{i,i}[\ell] \right|^2 + \left| \psi''_{i,i}[\ell] \right|^2 \right) \right.$$

$$\left. + \sum_{\substack{k=0 \\ k \neq i}}^{M-1} \sum_{\ell} \left(\left| \psi'_{i,k}[\ell]\cdot \right|^2 + \left| \psi''_{i,k}[\ell]\cdot \right|^2 \right) \right).$$

$$(24)$$

The noise power calculation is reported in Appendix B. Nonetheless, assuming that the PLC noise is AWGN, (B.7) and (B.8) can be simplified as follows

$$P_r^+ (i) = \sigma_r^2 \left(\sum_{t=0}^{N+2L_A} \left| h^{cc+}_{i,\mu}[t] + h^{ss+}_{i,\mu}[t] \right|^2 + \left| h^{cs+}_{i,\mu}[t] - h^{sc+}_{i,\mu}[t] \right|^2 \right), \qquad (25)$$

$$P_r^- (i) = \sigma_r^2 \left(\sum_{t=0}^{N+2L_A} \left| h^{cc-}_{i,\mu}[t] - h^{ss-}_{i,\mu}[t] \right|^2 + \left| h^{cs-}_{i,\mu}[t] + h^{sc-}_{i,\mu}[t] \right|^2 \right), \qquad (26)$$

where

$$h^{cc\pm}_{i,\mu}[n] = h_i^c[n] * c_k^\pm[n]; \qquad h^{ss\pm}_{i,\mu}[n] = h_i^s[n] * s_k^\pm[n]$$

$$h^{cs\pm}_{i,\mu}[n] = h_i^c[n] * s_k^\pm[n]; \qquad h^{sc\pm}_{i,\mu}[n] = h_i^s[n] * c_k^\pm[n]$$

With these above powers, the SINR can be calculated as [21]

$$\mathrm{SINR}^\pm (i) = \frac{P_\gamma^\pm (i)\, \sigma_x^2}{P^\pm_{ICI+ISI} (i) + P_r^\pm (i)}. \qquad (27)$$

Finally, the wavelet OFDM achievable data rate can be obtained as

$$T_R^\pm = \sum_{m=0}^{M-1} \Delta_f \cdot C^\pm(i), \qquad (28)$$

where Δ_f is the frequency spacing and $C^\pm(i)$ is the maximal data rate for the ith subcarrier, which can be calculated by means of the following expression [22, 23]:

$$C^\pm(i) = \log_2 \left(1 + \frac{\mathrm{SINR}^\pm(i)}{\chi} \right), \qquad (29)$$

where χ is the SINR gap. For $\chi = 1$, $C^{\pm}(i)$ is the capacity. Assuming PAM modulation, it is defined as:

$$\chi = \frac{1}{3}\left[Q^{-1}\left(\frac{SER}{2}\right)^2\right],\tag{30}$$

where SER is the symbol error rate and $Q^{-1}(\cdot)$ is the inverse tail probability of the standard normal distribution [22, 23]. In all our simulations χ has been fixed to 5.57 dB, leading to a target SER of 10^{-3}.

4. Simulation Results

In this section, the performance of the bandpass ELT-MCM system is analyzed in terms of bit-error-rate (BER) and data rate. The system is implemented with the following IEEE 1901 specifications. The number of subcarriers in positive and negative subbands is $M = 512$, with only 360 active subcarriers (M_{ac}) in the range of $[1.8 - 50]$ MHz. Additionally, the prototype filter is selected with $\kappa = 2$. The frequency spacing (Δ_f) equals 61.03515625 KHz. An error-correcting-code (ECC) system, which is based on the concatenated encoder[2] with a coding rate of $1/2$ [9, 14.3], has been also used to calculate the BER. Meanwhile, a non-ECC system has been employed to obtain the achievable data rate. The equalization process is carried out by 0-ASCET (1-tap), 1-ASCET (3-tap) or 2-ASCET (5-tap).

The in-home PLC channels are modeled following [24]. Particularly, a set of 100 realizations of the channel models: Class 9 (little signal attenuation), Class 5 (medium attenuation) and Class 1 (strong attenuation) [25], obtained by means of the script available on-line in [26], have been employed. Furthermore, it is assumed that the channel remains constant during each multicarrier symbol and that it is perfectly known at the receiver side.

For the simulations, the average Signal-to-Noise Ratio (SNR) is obtained from the receiver side as follows [21]:

$$\text{SNR}_{\text{RX}} = 10\log_{10}\left(\frac{1}{M_{ac}}\sum_{k\in\mathbb{K}_{on}}\frac{|H_k|^2\sigma_x^2(k)}{\sigma_n^2(k)}\right),\tag{31}$$

where H_k is the frequency channel coefficient and $\sigma_n^2(k)$ denotes the noise level at the k-th subcarrier. Furthermore, the noise in the PLC system consist of colored background noise (BGN), periodic impulsive noise synchronous and asynchronous to mains frequency (PINs), asynchronous impulsive noise (AIN) and narrowband interference (NBI) [27]. All of these noises have been modeled by the scripts that are available on-line in [28] according to the model presented in [29].

---

[2]The ECC consists of a Reed-Solomon enconder applied to the output data of the scrambler. Next, there is a second convolutional encoder. We refer the reader to [9, Sec. 14.3.4] for more details.
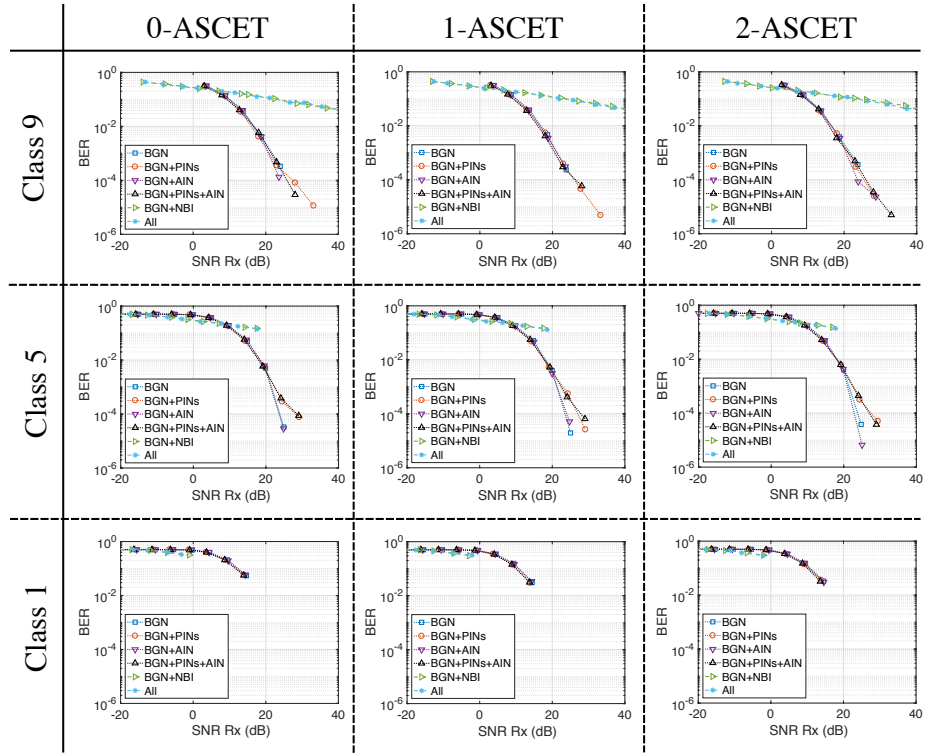
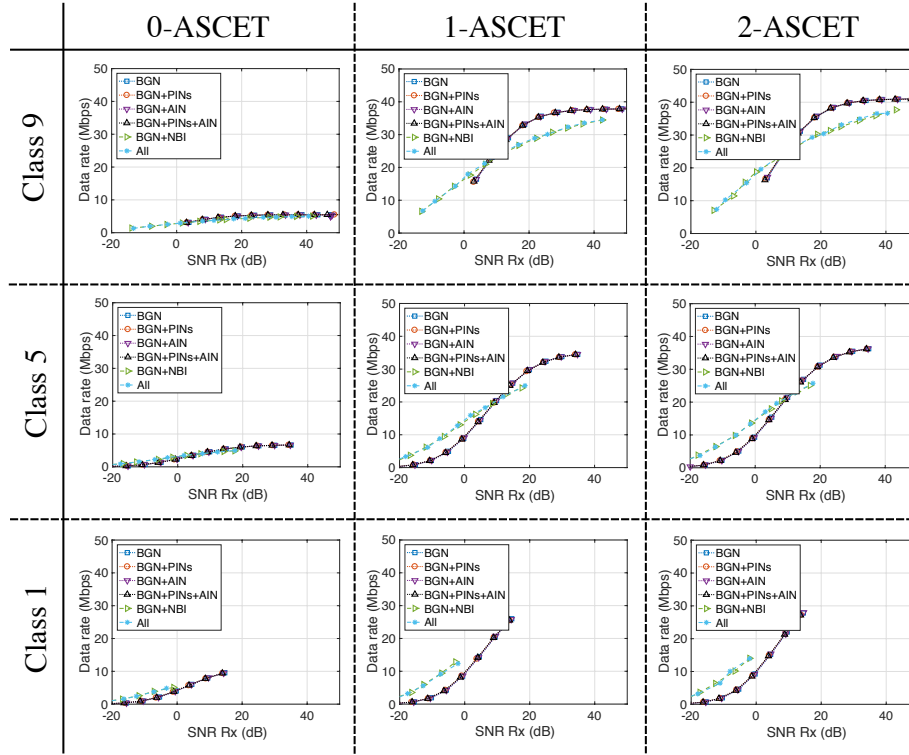Figure 4: BER for different in-home PLC channel, noises and equalizers.

Figure 5: Achievable data rate for different in-home PLC channel, noises and equalizers.

Fig. 4 depicts the BER obtained, under the above conditions for a BPSK (referred to as 2-PAM by the standard) modulation. As can be appreciated, the system achieves a very good performance even when PINs and AIN are added to BGN. Nevertheless, the system efficiency declines when NBI appears, even when the equalizer complexity is increased up to 5-tap (2-ASCET).

Fig. 5 shows the resulting data rate, considering a constellation of infinity granularity, and Table 1 summarizes the results obtained by each equalizer for SNR = 15 dB, considering either BGN or all kind of noises. It can be noticed that even though the performance in terms of BER is quite similar, the data rate achieved for the system increases when the equalizer complexity also increases. For instance, the ELT-MCM data rate associated with 2-ASCET is 605% higher than 0-ASCET and 8% greater than 1-ASCET for Class 9 and BGN, SNR = 15 dB. Nonetheless, these results suggest that the difference in data rate will be negligible if a more complex equalizer (e.g. 3-ASCET or higher) is used, therefore, a 2-ASCET could be a good ending point. Observe that there are some cases where the system is not able to reach a BER lower than 10^{-2}. This is due to the fact that the different impulse responses of the PLC channel models have not been normalized to unit total energy. In this sense, the Class 9 channel attenuates the transmitted signal by a factor equals to 8.5 dB, whereas Class 5 and Class 1 channels introduce attenuation of 30 dB and 60 dB, respectively [25].

In Table 1, the data rate of Class 1 channels with BGN is higher than the ones of Class 5, under the same noise and interference conditions. Note that in (27), the channel attenuation is a common factor affecting the powers of the signal, the ISI and the ICI, as well as the power of the noise. Thus, considering that the power of the interference is less than that of the useful signal, the smaller the values of the channel coefficients per subcarrier, the greater the SINR. The difference in the results obtained for Class 5 and Class 1 channels is smaller as the ASCET order increases, as the filtering of the per-subcarrier equalizer corrects this effect. Finally, Table 1 does not provide results of data rate for Class 1 channels under all noises since it was not possible for the receiver achieves an SNR = 15 dB. Class 1 channels present the highest attenuation, around 60 dB for frequencies between 0 and 100 MHz [25]. The system performance could be improved increasing the transmitted power, which is not a practical solution in real implementations, or applying noise reduction techniques. This study is out of the scope of this work.

5. Conclusion

This paper has presented some relevant aspects of the wavelet OFDM band-pass physical layer deployed by the IEEE P1901 working group for broadband communications over the power grid network. It has further proposed a viable system, transmitter and receiver with equalizer, based on the time-domain wave-form signals described in the standard. Likewise, the theoretical expressions to obtain the SINR and the achievable data rate have been derived. The desired signal power, the interference and the noise power have been calculated at the

Table 1: Results of data Rate for Different Noises (SNR= 15 dB).

	0-ASCET	1-ASCET	2-ASCET
Class 9			
Data rate with BGN (Mbps)	4.83	30.10	32.33
Data rate with all noises (Mbps)	4.02	26.08	28.11
Class 5			
Data rate with BGN (Mbps)	5.50	25.88	27.03
Data rate with all noises (Mbps)	4.74	23.16	24.30
Class 1			
Data rate with BGN (Mbps)	9.59	26	27.84
Data rate with all noises (Mbps)	−−	−−	−−

receiver side. It is important to highlight that the noise term has been derived assuming non-AWGN as PLC noise, which corresponds to a more realistic scenario. Finally, we have investigated the performance of the proposed system under several noises in the PLC system. Our simulation results confirm that this is able to deal with low and high frequency selective channels, considering different PLC scenarios.

Acknowledgments

Appendix A. Calculation of (18)

First, the real part is analyzed. Thus, the ith output of the analysis CMFB in the absence of noise can be obtained as

$$
\begin{aligned}
Y_i^{rc}(z) &= \frac{1}{M} \sum_{l \in \mathbb{K}_{on}} H_i^c \left(z^{\frac{1}{M}} W^l \right) \Re \left\{ Y \left(z^{\frac{1}{M}} W^l \right) \right\} \\
&= \frac{1}{M} \sum_{l \in \mathbb{K}_{on}} H_i^c \left(z^{\frac{1}{M}} W^l \right) \left[S^I \left(z^{\frac{1}{M}} W^l \right) \times H_{ch}^I \left(z^{\frac{1}{M}} W^l \right) \right. \\
&\quad \left. - S^Q \left(z^{\frac{1}{M}} W^l \right) H_{ch}^Q \left(z^{\frac{1}{M}} W^l \right) \right] \left(z^{\frac{1}{M}} W^l \right)^{-\beta} \\
&= \frac{1}{M} \sum_{l \in \mathbb{K}_{on}} H_i^c \left(z^{\frac{1}{M}} W^l \right) \\
&\quad \times \left[\sum_{k \in \mathbb{K}_{on}} F_k^c \left(z^{\frac{1}{M}} W^l \right) \left(X_k^+(z) - X_k^-(z) \right) H_{ch}^I \left(z^{\frac{1}{M}} W^l \right) \right. \\
&\quad \left. - \sum_{k \in \mathbb{K}_{on}} F_k^s \left(z^{\frac{1}{M}} W^l \right) \left(X_k^+(z) + X_k^-(z) \right) H_{ch}^Q \left(z^{\frac{1}{M}} W^l \right) \right] z^{-\frac{\beta}{M}} W^{-l\beta},
\end{aligned}
$$
(A.1)

where $W = e^{-j\frac{2\pi}{M}}$ and $H_k^c(z)$ is the z-transform of the filter given in (8a). Rearranging terms, and defining $T_{i,k}^{ccI}(z) = H_i^c(z) \cdot F_k^c(z) \cdot H_{ch}^I(z)$ and $T_{i,k}^{csQ}(z) = H_i^c(z) \cdot F_k^s(z) \cdot H_{ch}^Q(z)$, the previous expressions can be rewritten as

$$
\begin{aligned}
Y_i^{rc}(z) &= \frac{1}{M} \sum_{k \in \mathbb{K}_{on}} X_k^+(z) \sum_{l \in \mathbb{K}_{on}} T_{i,k}^{ccI} \left(z^{\frac{1}{M}} W^l \right) z^{-\frac{\beta}{M}} W^{-l\beta} \\
&\quad - \frac{1}{M} \sum_{k \in \mathbb{K}_{on}} X_k^+(z) \sum_{l \in \mathbb{K}_{on}} T_{i,k}^{csQ} \left(z^{\frac{1}{M}} W^l \right) z^{-\frac{\beta}{M}} W^{-l\beta} \\
&\quad - \frac{1}{M} \sum_{k \in \mathbb{K}_{on}} X_k^-(z) \sum_{l \in \mathbb{K}_{on}} T_{i,k}^{ccI} \left(z^{\frac{1}{M}} W^l \right) z^{-\frac{\beta}{M}} W^{-l\beta} \\
&\quad - \frac{1}{M} \sum_{k \in \mathbb{K}_{on}} X_k^-(z) \sum_{l \in \mathbb{K}_{on}} T_{i,k}^{csQ} \left(z^{\frac{1}{M}} W^l \right) z^{-\frac{\beta}{M}} W^{-l\beta} \\
&= \sum_{k \in \mathbb{K}_{on}} X_k^+(z) \left(U_{i,k}^{ccI}(z) - U_{i,k}^{csQ}(z) \right) \\
&\quad + \sum_{k \in \mathbb{K}_{on}} X_k^-(z) \left(-U_{i,k}^{ccI}(z) - U_{i,k}^{csQ}(z) \right),
\end{aligned}
$$
(A.2)

where the relation in the time-domain between $U(z)$ and $T(z)$ is given by $u_{i,k}^{ccI}[n] = t_{i,k}^{ccI}[nM - \beta]$ and $u_{i,k}^{csQ}[n] = t_{i,k}^{csQ}[nM - \beta]$. It is important to note that when the subchannel filters show both high selectivity and discrimination between subcarriers, the functions $t_{i,k}^{ccI}[nM - \beta]$ and $t_{i,k}^{csQ}[nM - \beta]$ are nearly zero for $k \neq \{i-1, i, i+1\}$.

Applying the same reasoning of the previous steps, the ith output of the real part of analysis SMFB, in the absence of noise, yields

$$Y_i^{rs}(z) = \sum_{k \in \mathbb{K}_{on}} X_k^+(z) \left(-U_{i,k}^{scI}(z) + U_{i,k}^{ssQ}(z) \right)$$
$$+ \sum_{k \in \mathbb{K}_{on}} X_k^-(z) \left(U_{i,k}^{scI}(z) + U_{i,k}^{ssQ}(z) \right), \tag{A.3}$$

where $H_k^s(z)$ is the z-transform of the filter given in (8a), and $T_{i,k}^{scI}(z) = H_i^s(z) \cdot F_k^c(z) \cdot H_{ch}^I(z)$, $T_{i,k}^{ssQ}(z) = H_i^s(z) \cdot F_k^s(z) \cdot H_{ch}^Q(z)$, $u_{i,k}^{scI}[n] = t_{i,k}^{scI}[nM - \beta]$ and $u_{i,k}^{ssQ}[n] = t_{i,k}^{ssQ}[nM - \beta]$.

Once the real part has been analyzed, the same study must be applied to the imaginary part. Therefore, the ith output of the analysis CMFB and SMFB, in the absence of noise, can be written as

$$Y_i^{\iota c}(z) = \sum_{k \in \mathbb{K}_{on}} X_k^+(z) \left(-U_{i,k}^{ccQ}(z) - U_{i,k}^{csI}(z) \right)$$
$$+ \sum_{k \in \mathbb{K}_{on}} X_k^-(z) \left(U_{i,k}^{ccQ}(z) - U_{i,k}^{csI}(z) \right), \tag{A.4}$$

where $T_{i,k}^{ccQ}(z) = H_i^c(z) \cdot F_k^c(z) \cdot H_{ch}^Q(z)$, $T_{i,k}^{csI}(z) = H_i^c(z) \cdot F_k^s(z) \cdot H_{ch}^I(z)$, $u_{i,k}^{ccQ}[n] = t_{i,k}^{ccQ}[nM - \beta]$ and $u_{i,k}^{csI}[n] = t_{i,k}^{csI}[nM - \beta]$. In addition, we have that

$$Y_i^{\iota s}(z) = \sum_{k \in \mathbb{K}_{on}} X_k^+(z) \left(U_{i,k}^{scQ}(z) + U_{i,k}^{ssI}(z) \right)$$
$$+ \sum_{k \in \mathbb{K}_{on}} X_k^-(z) \left(-U_{i,k}^{scQ}(z) + U_{i,k}^{ssI}(z) \right), \tag{A.5}$$

where $T_{i,k}^{scQ}(z) = H_i^s(z) \cdot F_k^c(z) \cdot H_{ch}^Q(z)$, $T_{i,k}^{ssI}(z) = H_i^s(z) \cdot F_k^s(z) \cdot H_{ch}^I(z)$, $u_{i,k}^{scQ}[n] = t_{i,k}^{scQ}[nM - \beta]$ and $u_{i,k}^{ssI}[n] = t_{i,k}^{ssI}[nM - \beta]$. By adding (A.2) and (A.5), it is obtained that

$$\alpha_i(z) = Y_i^{rc}(z) + Y_i^{\iota s}(z)$$
$$= \sum_{k \in \mathbb{K}_{on}} X_k^+(z) \left(U_{i,k}^{ccI}(z) - U_{i,k}^{csQ}(z) + U_{i,k}^{scQ}(z) + U_{i,k}^{ssI}(z) \right)$$
$$+ \sum_{k \in \mathbb{K}_{on}} X_k^-(z) \left(-U_{i,k}^{ccI}(z) - U_{i,k}^{csQ}(z) - U_{i,k}^{scQ}(z) + U_{i,k}^{ssI}(z) \right)$$
$$= \sum_{k \in \mathbb{K}_{on}} X_k^+(z) \alpha'_{i,k}(z) + \sum_{k \in \mathbb{K}_{on}} X_k^-(z) \alpha''_{i,k}(z). \tag{A.6}$$

In the same way, we get

$$\beta_i(z) = Y_i^{rs}(z) - Y_i^{\iota c}(z)$$
$$= \sum_{k \in \mathbb{K}_{on}} X_k^+(z) \beta'_{i,k}(z) + \sum_{k \in \mathbb{K}_{on}} X_k^-(z) \beta''_{i,k}(z). \tag{A.7}$$

$$\gamma_i(z) = Y_i^{rs}(z) + Y_i^{\iota c}(z) = \sum_{k \in \mathbb{K}_{on}} X_k^+(z)\gamma_{i,k}'(z) + \sum_{k \in \mathbb{K}_{on}} X_k^-(z)\gamma_{i,k}''(z), \quad \text{(A.8)}$$

$$\varepsilon_i(z) = -Y_i^{rc}(z) + Y_i^{\iota s}(z) = \sum_{k \in \mathbb{K}_{on}} X_k^+(z)\varepsilon_{i,k}'(z) + \sum_{k \in \mathbb{K}_{on}} X_k^-(z)\varepsilon_{i,k}''(z). \quad \text{(A.9)}$$

Next, assuming that an L_A-ASCET is chosen as channel equalization technique, the ith demodulated symbol of the positive $(+)$ and negative $(-)$ subband can be written as

$$\begin{aligned}
\hat{X}_i^+(z) &= \alpha_{i,k}(z)C_i^+(z) + \beta_{i,k}(z)S_i^+(z) \\
&= \sum_{k \in \mathbb{K}_{in}} X_k^+(z)\left(\alpha_{i,k}'(z)C_i^+(z) + \beta_{i,k}''(z)S_i^+(z)\right) \\
&\quad + \sum_{k \in \mathbb{K}_{in}} X_k^-(z)\left(\alpha_{i,k}''(z)C_i^+(z) + \beta_{i,k}''(z)S_i^+(z)\right) \\
&= \sum_{k \in \mathbb{K}_{in}} X_k^+(z)\Upsilon_{i,k}'(z) + \sum_{k \in \mathbb{K}_{in}} X_k^-(z)\Upsilon''_{i,k}(z), \quad \text{(A.10)}
\end{aligned}$$

and

$$\begin{aligned}
\hat{X}_i^-(z) &= \gamma_{i,k}(z)S_i^-(z) + \varepsilon_{i,k}(z)C_i^-(z) \\
&= \sum_{k \in \mathbb{K}_{in}} X_k^+(z)\left(\gamma_{i,k}'(z)C_i^+(z) + \varepsilon_{i,k}''(z)S_i^+(z)\right) \\
&\quad + \sum_{k \in \mathbb{K}_{in}} X_k^-(z)\left(\gamma_{i,k}''(z)C_i^+(z) + \varepsilon_{i,k}''(z)S_i^+(z)\right) \\
&= \sum_{k \in \mathbb{K}_{in}} X_k^+(z)\Psi_{i,k}'(z) + \sum_{k \in \mathbb{K}_{in}} X_k^-(z)\Psi''_{i,k}(z), \quad \text{(A.11)}
\end{aligned}$$

where $C_i^\pm$ and $S_i^\pm$ are, respectively, the z-transform of

$$c_i^\pm[n] = \sum_{\mu=-L_A}^{L_A} c_{i,\mu}^\pm \cdot \delta[n-\mu], \quad \text{(A.12a)}$$

$$s_i^\pm[n] = \sum_{\mu=-L_A}^{L_A} s_{i,\mu}^\pm \cdot \delta[n-\mu], \quad \text{(A.12b)}$$

with $c_i[n]$ and $s_i[n]$ being the impulse response of the subcarrier filters that carry out the frequency domain equalization.

Appendix B. Noise power calculation

With regard to the noise at the ith output of the analysis CMFB/SMFB, related to the real and imaginary part, can be obtained as

$$r_i^{rc}[n] = \sum_t h_i^c[t] \cdot r_I[nM - t - \beta], \quad \text{(B.1)}$$

$$r_i^{rs}[n] = \sum_t h_i^s[t] \cdot r_I \left[nM - t - \beta \right], \tag{B.2}$$

$$r_i^{\iota c}[n] = \sum_t h_i^c[t] \cdot r_Q \left[nM - t - \beta \right], \tag{B.3}$$

$$r_i^{\iota s}[n] = \sum_t h_i^s[t] \cdot r_Q \left[nM - t - \beta \right]. \tag{B.4}$$

Therefore, the noise at the ith demodulated symbol of the positive subbands is

$$r_i^+[n] = \sum_{\mu=-L_A}^{L_A} c_{i,\mu} \left(r_i^{rc}[n-\mu] + r_i^{\iota s}[n-\mu] \right) + s_{i,\mu} \left(r_i^{rs}[n-\mu] - r_i^{\iota c}[n-\mu] \right), \tag{B.5}$$

whereas that of the negative subbands is given by

$$r_i^-[n] = \sum_{\mu=-L_A}^{L_A} c_{i,\mu} \left(-r_i^{rc}[n-\mu] + r_i^{\iota s}[n-\mu] \right) + s_{i,\mu} \left(r_i^{rs}[n-\mu] + r_i^{\iota c}[n-\mu] \right). \tag{B.6}$$

Therefore, the noise power yields

$$
\begin{aligned}
P_r^+(i) = &\sum_{\mu_1=-L_A}^{L_A} \sum_{\mu_2=-L_A}^{L_A} \left[\sum_{t_1} \sum_{t_2} R_{RII} \left(t_1 + \mu_1 M, t_2 + \mu_2 M \right) \right. \\
& \left(c_{i,\mu_1}^+ c_{i,\mu_2}^+ h_i^c[t_1] h_i^c[t_2] + s_{i,\mu_1}^+ s_{i,\mu_2}^+ h_i^s[t_1] h_i^s[t_2] + 2 c_{i,\mu_1}^+ s_{i,\mu_2}^+ h_i^c[t_1] h_i^s[t_2] \right) \Bigg] \\
& + 2 \sum_{\mu_1=-L_A}^{L_A} \sum_{\mu_2=-L_A}^{L_A} \left[\sum_{t_1} \sum_{t_2} R_{RIQ} \left(t_1 + \mu_1 M, t_2 + \mu_2 M \right) \right. \\
& \left(c_{i,\mu_1}^+ c_{i,\mu_2}^+ h_i^c[t_1] h_i^s[t_2] - c_{i,\mu_1}^+ s_{i,\mu_2}^+ h_i^c[t_1] h_i^c[t_2] \right. \\
& \left. + s_{i,\mu_1}^+ c_{i,\mu_2}^+ h_i^s[t_1] h_i^s[t_2] - s_{i,\mu_1}^+ s_{i,\mu_2}^+ h_i^s[t_1] h_i^c[t_2] \right) \Bigg]. \\
& + \sum_{\mu_1=-L_A}^{L_A} \sum_{\mu_2=-L_A}^{L_A} \left[\sum_{t_1} \sum_{t_2} R_{RQQ} \left(t_1 + \mu_1 M, t_2 + \mu_2 M \right) \right. \\
& \left(c_{i,\mu_1}^+ c_{i,\mu_2}^+ h_i^s[t_1] h_i^s[t_2] + s_{i,\mu_1}^+ s_{i,\mu_2}^+ h_i^c[t_1] h_i^c[t_2] - 2 c_{i,\mu_1}^+ s_{i,\mu_2}^+ h_i^s[t_1] h_i^c[t_2] \right) \Bigg],
\end{aligned}
\tag{B.7}
$$

$$P_r^-(i) = \sum_{\mu_1=-L_A}^{L_A} \sum_{\mu_2=-L_A}^{L_A} \left[\sum_{t_1} \sum_{t_2} R_{RII}\left(t_1 + \mu_1 M, t_2 + \mu_2 M\right) \right.$$

$$\left. \left(c_{i,\mu_1}^- c_{i,\mu_2}^- h_i^c[t_1]h_i^c[t_2] + s_{i,\mu_1}^- s_{i,\mu_2}^- h_i^s[t_1]h_i^s[t_2] - 2c_{i,\mu_1}^- s_{i,\mu_2}^- h_i^c[t_1]h_i^s[t_2]\right) \right]$$

$$+ 2 \sum_{\mu_1=-L_A}^{L_A} \sum_{\mu_2=-L_A}^{L_A} \left[\sum_{t_1} \sum_{t_2} R_{RIQ}\left(t_1 + \mu_1 M, t_2 + \mu_2 M\right) \right.$$

$$\left(-c_{i,\mu_1}^- c_{i,\mu_2}^- h_i^c[t_1]h_i^s[t_2] - c_{i,\mu_1}^- s_{i,\mu_2}^- h_i^c[t_1]h_i^c[t_2]\right.$$

$$\left.\left. + s_{i,\mu_1}^- c_{i,\mu_2}^- h_i^s[t_1]h_i^s[t_2] + s_{i,\mu_1}^- s_{i,\mu_2}^- h_i^s[t_1]h_i^c[t_2]\right) \right].$$

$$+ \sum_{\mu_1=-L_A}^{L_A} \sum_{\mu_2=-L_A}^{L_A} \left[\sum_{t_1} \sum_{t_2} R_{RQQ}\left(t_1 + \mu_1 M, t_2 + \mu_2 M\right) \right.$$

$$\left.\left(c_{i,\mu_1}^- c_{i,\mu_2}^- h_i^s[t_1]h_i^s[t_2] + s_{i,\mu_1}^- s_{i,\mu_2}^- h_i^c[t_1]h_i^c[t_2] + 2c_{i,\mu_1}^- s_{i,\mu_2}^- h_i^s[t_1]h_i^c[t_2]\right) \right],$$

$$\text{(B.8)}$$

where

$$R_{RII}\left(t_1 + \mu_1 M, t_2 + \mu_2 M\right) = E\left[r_I\left[(n-\mu_1)M - t_1 - \beta\right]\right.$$
$$\left.\times r_I\left[(n-\mu_2)M - t_2 - \beta\right]\right], \qquad \text{(B.9)}$$

$$R_{RIQ}\left(t_1 + \mu_1 M, t_2 + \mu_2 M\right) = E\left[r_I\left[(n-\mu_1)M - t_1 - \beta\right]\right.$$
$$\left.\times r_Q\left[(n-\mu_2)M - t_2 - \beta\right]\right], \qquad \text{(B.10)}$$

$$R_{RQQ}\left(t_1 + \mu_1 M, t_2 + \mu_2 M\right) = E\left[r_Q\left[(n-\mu_1)M - t_1 - \beta\right]\right.$$
$$\left.\times r_Q\left[(n-\mu_2)M - t_2 - \beta\right]\right], \qquad \text{(B.11)}$$

with $E\left[\cdot\right]$ being the expected value. Assuming that the PLC noise is a stationary stochastic processes, $R_R(t_1 + \mu_1 M, t_2 + \mu_2 M)$ can be rewritten as $R_R(\tau)$ being $\tau = (t_2 - t_1) + M(\mu_2 - \mu_1)$.

References

[1] S. Galli, A. Scaglione, Z. Wang, For the grid and through the grid: The role of power line communications in the smart grid, Proceedings of the IEEE 99 (6) (2011) 998–1027.

[2] M. P. Tcheou, L. Lovisolo, M. V. Ribeiro, E. A. B. da Silva, M. Rodrigues, J. M. T. Romano, P. S. R. Diniz, The compression of electric signal waveforms for smart grids: State of the art and future trends, IEEE Transactions on Smart Grid 5 (1) (2014) 291–302. `doi:10.1109/TSG.2013.2293957`.

[3] R. Ma, H.-H. Chen, Y.-R. Huang, W. Meng, Smart grid communication: Its challenges and opportunities, IEEE Transactions on Smart Grid 4 (1) (2013) 36–46. `doi:10.1109/TSG.2012.2225851`.

[4] A. Zanella, N. Bui, A. Castellani, L. Vangelista, M. Zorzi, Internet of things for smart cities, IEEE Internet of Things Journal 1 (1) (February 2014) 22–32.

[5] S. Barker, D. Irwin, P. Shenoy, Pervasive energy monitoring and control through low-bandwidth power line communication, IEEE Internet of Things Journal 4 (5) (2017) 1349–1359. `doi:10.1109/JIOT.2017.2703916`.

[6] L. D. M. B. A. Dib, V. Fernandes, M. D. L. Filomeno, M. V. Ribeiro, Hybrid plc/wireless communication for smart grids and internet of things applications, IEEE Internet of Things Journal 5 (2) (2018) 655–667. `doi:10.1109/JIOT.2017.2764747`.

[7] X. Li, R. Lu, X. Liang, X. Shen, J. Chen, X. Lin, Smart community: An internet of things application, IEEE Communications Magazine 49 (11) (November 2011) 68–75.

[8] Y. Qian, J. Yan, H. Guan, J. Li, X. Zhou, S. Guo, D. N. K. Jayakody, Design of hybrid wireless and power line sensor networks with dual-interface relay in IoT, IEEE Internet of Things Journal (Early Access).

[9] IEEE Std 1901-2010, IEEE standard for broadband over power line networks: Medium access control and physical layer specifications (2010) 1–1586`doi:10.1109/IEEESTD.2010.5678772`.

[10] IEEE Standard for Low-Frequency (less than 500 kHz) Narrowband Power Line Communications for Smart Grid Applications.

[11] F. Cruz-Roldán, F. A. Pinto-Benel, J. Osés del Campo, M. Blanco-Velasco, A wavelet OFDM receiver for baseband power line communications, Journal of the Franklin Institute 353 (7) 1654–1671.

[12] F. A. Pinto-Benel, F. Cruz-Roldán, Exploring the performance of prototype filters for broadband PLC, in: IEEE International Symposium on Power Line Communications and its Applications (ISPLC), 2017, 2017.

[13] A. Viholainen, Modulated filter bank design for communication signal processing, Ph.D. thesis, Tampere University of Technology (2004).

[14] T. Ihalainen, T. H. Stitz, M. Renfors, Efficient per-carrier channel equalizer for filter bank based multicarrier systems, in: Proc. Int. Symp. on Circuits and Systems, Kobe, Japan, May 2005, pp. 3175 –3178.

[15] A. Viholainen, J. Alhava, M. Renfors, Efficient implementation of complex modulated filter banks using cosine and sine modulated filter banks, EURASIP Journal on Applied Signal Processing 2006 (2006) Article ID 58564, 10 pages.

[16] T. Ihalainen, T. Hidalgo Stitz, M. Rinne, M. Renfors, Channel equalization in filter bank based multicarrier modulation for wireless communications, EURASIP Journal on Advances in Signal Processing 2007.

[17] J. Alhava, M. Renfors, Adaptive sine-modulated/cosine-modulated filter bank equalizer for transmultiplexers, in: Proc. European Conference on Circuit Theory and Design, Espoo, Finland, August 2001, pp. 337–340.

[18] K. Izumi, D. Umehara, S. Denno, Performance evaluation of wavelet OFDM using ASCET, in: Proc. 17th IEEE International Symposium on Power Line Communications and Its Applications, Pisa, Italy, March 2007, pp. 246–251.

[19] F. A. Pinto-Benel, F. Cruz-Roldán, 2-ASCET for broadband multicarrier transmission over in-home and in-vehicle power line networks, in: IEEE 18th International Conference on Intelligent Transportation Systems, 2015, pp. 1351 – 1356.

[20] Y. Yang, T. Ihalainen, M. Rinne, M. Renfors, Frequency-domain equalization in single-carrier transmission: filter bank approach, EURASIP Journal on Advances in Signal Processing 2007 (1) (2007) 135–135.

[21] P. Achaichia, M. L. Bot, P. Siohan, OFDM/OAQM: A solution to efficiently increase the capacity of future PLC networks, IEEE Transactions on Power Delivery 26 (4) (2011) 2443–2455.

[22] J. Cioffi, Digital Communications, chap. 4: Multichannel Modulation., https://web.stanford.edu/group/cioffi/doc/book/chap4.pdf.

[23] S. D. Sandberg, M. A. Tzannes, Overlapped discrete multitone modulation for high speed copper wire communications, IEEE Journal on Selected Areas in Communications 13 (1995) 1571–1585.

[24] A. M. Tonello, S. D'Alessandro, L. Lampe, Cyclic prefix design and allocation in bit-loaded OFDM over power line communication channels, IEEE Transactions on Communication 58 (11) (November 2010) 3265–3276.

[25] Seventh Framework Programme: Theme 3 ICT-213311 OMEGA, PLC channel and modelling, Tech. rep., http://www.ict-omega.eu/ (2008).

[26] A. Tonello, Brief tutorial on the statistical top-down PLC channel generator, http://www.diegm.uniud.it/tonello/plcresearch.html (2010).

[27] M. Zimmermann, K. Doster, Analysis and modeling of impulsive noise in broadband powerline communications, IEEE Transactions on electromagnetic compatibility 44 (1) (February 2002) 249–258.

[28] L. Lampe, A cumulative power line noise generator, http://www.ece.ubc.ca/ gauthamp/PLCnoise/.

[29] G. Prasad, L. Lampe, S. Shekhar, In-band full duplex broadband power line communications, IEEE Transactions on Communications 64 (9) (2016) 3915–3931.